PERIODIC PROGRESS REPORT NO. 2

FOR

STUDY OF COMMUNICATIONS SYSTEMS, AND DETECTION AND TRACKING SYSTEMS.

DESIGN AND FABRICATION OF DYNAMIC CROSSED-FIELD ELECTRON-MULTIPLYING LIGHT DEMODULATOR.

20 JUNE 1964 TO 20 SEPTEMBER 1964

Contract No.: NAS5-3777

Prepared by

The Hallicrafters Co.
5th and Kostner Avenues
Chicago 24, Illinois

for

Goddard Space Flight Center

Greenbelt, Maryland

PERIODIC PROGRESS REPORT NO. 2

FOR

STUDY OF COMMUNICATIONS SYSTEMS, AND DETECTION AND TRACKING SYSTEMS

DESIGN AND FABRICATION OF DYNAMIC CROSSED-FIELD ELECTRON MULTIPLYING LIGHT DEMODULATOR

20 JUNE 1964 TO 20 SEPTEMBER 1964

Contract No.: NAS5-3777

Prepared by

M. Ross
R. Hankin
E. Dallafior
R. Swendsen
T. Curran

The Hallicrafters Co.
5th and Kostner Avenues
Chicago 24, Illinois

for

Goddard Space Flight Center

Greenbelt, Maryland

ABSTRACT

This second quarterly report presents results of an optical communications and tracking systems program divided into three specific Tasks as follows:

Task I: Analyze laser communications, detection, and tracking systems

Task II: Disseminate the results of Task I through a lecture series, and

Task III: Develop a microwave bandwidth dynamic crossed-field electron multiplier demodulator.

Work in the second quarter is reported for all three tasks.

Task I results for the second quarter include an analysis of laser receiver statistics and noise, a further analysis of the utilization of the Goddard Range and Range Rate System on an optical carrier, a summary of noise sources with a discussion of origin and effect, and an analysis of information theory aspects wherein quantum effects at optical frequencies are considered. Equations, charts, and graphs are provided.

Five lectures were given under Task II in the second quarter. Subject matter included radiation laws and statistics, noise and fluctuations, detection statistics, and information theory aspects.

Task III results for the second quarter include construction of cylindrical geometry dynamic crossed-field electron multiplier light demodulators and preliminary measurements of frequency response. Frequency response was indicated to at least 1 KMC. Photo-beats up to 600 MC have been detected from a gas laser source. Ultimate frequency response has not been experimentally determined. Delivery of an experimental tube will be accomplished within the next reporting period.

Author

TABLE OF CONTENTS

TABLE OF CONTENTS (CONT)

LIST OF ILLUSTRATIONS

1. TASK I EFFORT

1.1 Introduction

Task I of the overall program relating to optical communication and tracking systems is a study devoted to theoretical analysis of communications, detection, and tracking systems. Task I will include work as specified below.

A. Emphasize thermal and quantum fluctuations under various conditions and relate microwave noise theory to optical noise theory and the statistical nature of fluctuations.

B. Include an analysis of photomixing and direct photo-detection techniques in light of NASA objectives and component state-of-the-art to deduce the minimum noise system for various conditions.

C. Perform a noise analysis of various optical receiving devices in different system configurations in order to establish the minimum noise system for a variety of conditions.

D. Study the effects of the input optical bandwidth and the post detection bandwidth upon system sensitivity.

E. Study the relationship of noise to coherence.

F. Perform a specific noise study concerning the dynamic crossed-field electron multiplier.

Work in the second quarter has been concerned with an analysis of noise sources in laser systems. Noise considerations are related to receiving systems and the Goddard Range and Range Rate System. A comprehensive summary of noise sources is given and aspects of information theory are examined.

1.2 Discussion

1.2.1 Laser Receiver Statistics And Noise

Although Poisson statistics are usually assumed at the optical receiver, this may not necessarily be true in special cases where a highly coherent laser is employed as the transmitter. The Poisson statistics result from non-coherent or black body radiation. Lasers which are highly coherent will have emission statistics different from that of a black body. The exact nature of these statistics have not been satisfactorily determined, however, it is clear that if the photon fluctuation statistics at the laser transmitter are substantially different from that of a black body signal, photon fluctuations at the receiver will also be different.

The photon degeneracy of lasers, that is the number of photons in each quantum state, is greater than unity, thus much greater wave interaction (thermal) noise will take place than for a black body.

It appears that the photon fluctuations would be that of black body photon fluctuations at RF where, $\overline{(\Delta \bar{n})^2} = \bar{n}^2$, except for the limiting output of the laser. This limiting action, also denoted as wave-amplitude stabilization,

tends to substantially reduce the amount of fluctuations. Thus, the photon fluctuations at the laser transmitter will be somewhere in between the two cases of $\overline{\Delta n^2} = \bar{n}^2$ and $\overline{\Delta n^2} = \bar{n}$; the latter case being that of a non-coherent optical source.

Yet, the theoretical quantum limitation or sensitivity may not be seriously affected. It can be considered that the fluctuation in time Δt will be a time-varying Poisson process with the time variation a random process related to bandwidth of the source. As the fluctuation [1,2] is given for

$$B_o >> \frac{1}{\Delta t}$$

$$\overline{\Delta n^2} = \bar{n} \left[1 + \frac{\bar{n}}{\Delta t \; B_o} \right]$$

In post-detection bandwidth terms

$$\overline{\Delta n^2} = \bar{n} \left\{ 1 + \bar{n} \left[\frac{2 B_d}{B_o} \right] \right\}$$

It is seen that if the received photon rate per measurement interval ($\bar{n}/\Delta t$) is small compared to B_o, that the detected fluctuations are Poisson in character. With highly coherent lasers the transmitted spectral bandwidth can approach the post-detection bandwidth (1) and wave interaction noise can occur.

The non-coherent background statistics will remain Poisson and the detection statistics will involve the combination of Poisson and the modified Poisson due to the laser radiation.

Some insight into this effect on the sensitivity with a time-varying Poisson process can be provided by the following argument:

Consider the receiver far enough away from the laser source that very few signal photons per measurement interval arrive. To be specific let us assume that the average number is 6. If the laser source has average fluctuations in photons in the measurement time such that the number of average transmitted photons per measurement interval varies between $\bar{n}$ and $2\bar{n}$, then at the receiver, the random variation will be such that between 4 and 8 average photons will be randomly received. We continue this rough line of reasoning and note that we will consider this time-varying Poisson distribution to be in the extreme, specifically two Poisson distributions, one of average $\bar{n}_s = 4$ and the other of average $\bar{n}_s = 8$. The probability of receiving one distribution or the other is then equally likely and random. If we now plot the two cumulative distributions, sum them point by point and compare it to the Poisson distribution for $\bar{n}_s = 6$, we can obtain a reason-

(1) There is no point in having the spectral bandwidth less than the post-detection bandwidth. The minimum spectral bandwidth B_o should be twice the post-detection bandwidth, if the laser is an ideal source with information bandwidth $B_o/2$.

able idea of the influence of the laser wave interaction noise at these low signal levels. (See Figure 1).

It is seen that the resultant distribution has somewhat greater spread than the Poisson distribution for $\bar{n}_s = 6$. Thus the error rates will increase but the increase does not appear significant as noted by the values of P_{ND} for n-- = 1 for the two cases of Poisson and laser-Modified (time-varying) Poisson. $P_{ND} = .002$ for the Poisson case, $P_{ND} = .009$ for the modified case. To state it another way, for the Poisson case, a $P_{ND} = .009$ can be attained for $n = 4.7$. Thus, for this example a highly coherent laser would at worst require an increase in received power of approximately 20% (about 1 DB) compared to the non-coherent source.

Experimental evidence to date has not found any significant noise due to the laser above the normally induced signal shot noise.

The important point of the above is that it would appear that use of a coherent laser as a source will not increase the received noise very much, if at all, over that of a non-coherent source for the same low level signal received. In fact, when one considers the additional noise upon detection that can result due to the finite bandwidth of the carrier, it is more correct to be concerned that the noise bandwidth of the carrier is not of the same order as the information bandwidth. The non-coherent laser bandwidth, if it is of the same order as the information bandwidth, will upon detection induce significant additional noise and thereby seriously degrade the signal-noise ratio. A mathematical analysis and figures are shown in Section 1.2.2. As the curves show, if the noise bandwidth is much greater than the information bandwidth, less degradation occurs. It is of value to explain this.

The carrier power we assume is constant. If the power is spread over a narrow spectrum such that the spectrum width equals the detection bandwidth (see Figure 2a), then beats will occur between different spectral components that will be amplified since it is within the detection bandwidth. If this same carrier power is spread over a much greater bandwidth (see Figure 2b) then less beats can occur between components that will result in frequency differences within the detection bandwidth. In addition, these beats will be less intense because each spectral component is reduced in power. Thus, the smaller the ratio of information bandwidth to carrier bandwidth, the less noise effects the non-coherent source will cause.

This essentially means that in any system, the laser source must be chosen with regard to the information bandwidth to be used.

1.2.2 Analysis of the Utilization of the Goddard Range and Range Rate System on an Optical Carrier

In the last periodic report, it was pointed out that there are two distinctly different ways of applying the Goddard Range and Range Rate System to an optical carrier. One is direct substitution of the present microwave carrier for the optical carrier. The other is modulation of the optical beam by the range and range rate system including the microwave carrier, which would then be a sub-carrier. Both systems require analysis to determine under what conditions it would be possible to operate.

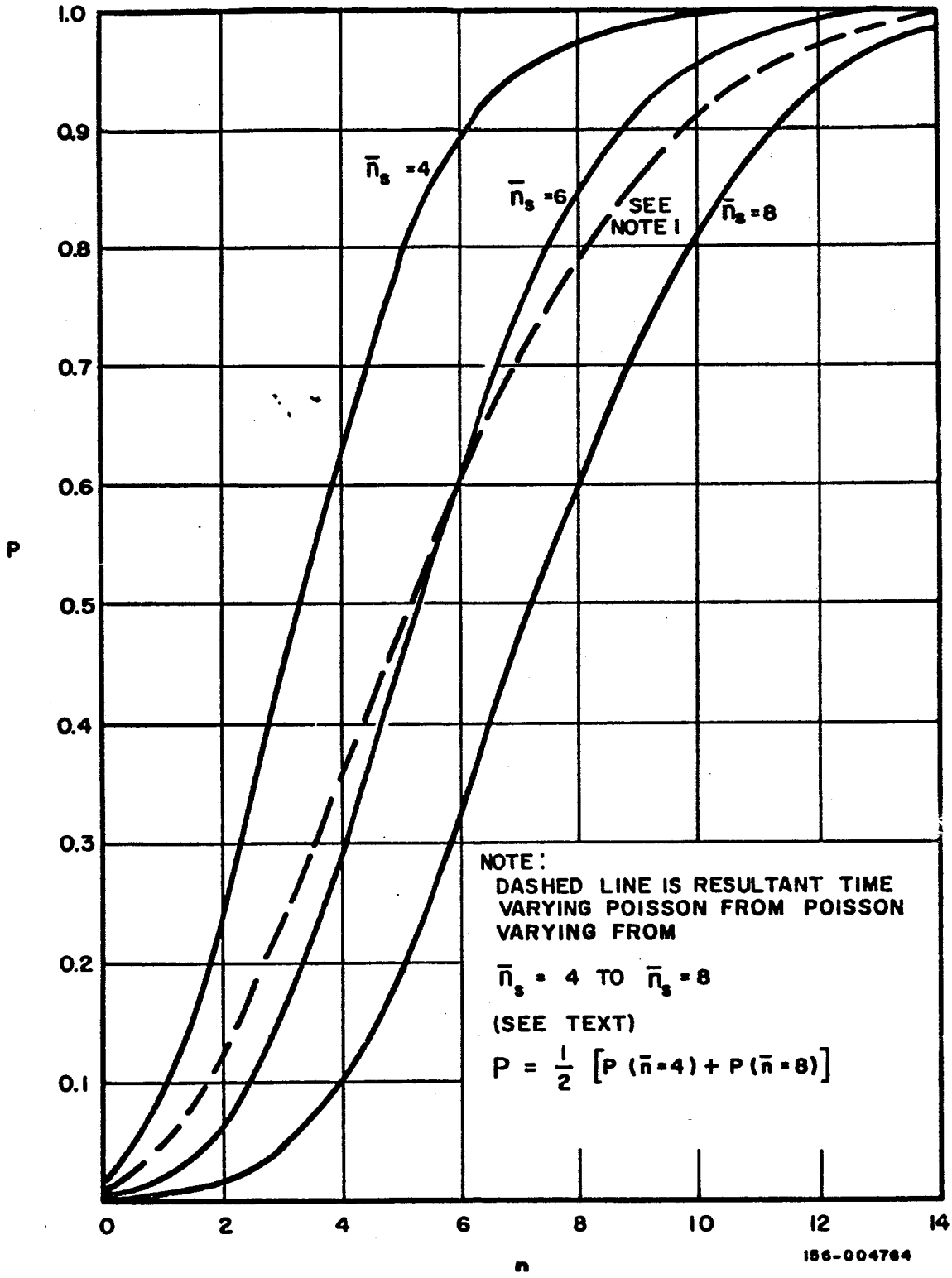

Figure 1. Comparison of Cumulative Distributions For Poisson and Time-Varying Poisson For $\bar{n}_s = 6$

It was pointed out in the last report that the noise bandwidth (or spectral coherence) of the optical carrier would play a significant role in determination of the feasibility of using the Goddard Range and Range Rate System. It was shown that it is necessary to determine the signal-to-noise degradation that will occur due to detection of the optical signal based upon the noise bandwidth of the carrier, the information bandwidth, and the highest sub-carrier frequency. There are two important conditions for the amplitude-modulated situation.

A. Baseband condition - where the highest modulation frequencies including sub-carrier are less than the carrier noise bandwidth.

B. Sub-carrier condition - where although the information bandwidth is less than the carrier noise bandwidth, the sub-carrier employed is much greater than the noise bandwidth.

In this report, a mathematical analysis of condition (A) baseband, is presented for the first time for the square law detector case which is the true situation at low signal levels for photon detectors such as photo-multipliers, photodiodes and photoconductors. The analysis for condition (B) specified above will be forthcoming in the next report.

Rowe has treated the linear detection of an amplitude modulated noise carrier. The following analysis extends his work to full wave square law detection of an amplitude modulated noise carrier.

Consider the AM system shown in Figure 3.

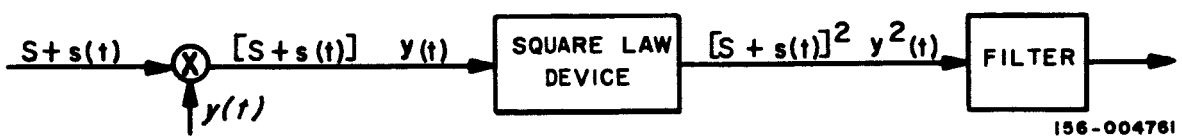

Figure 3. - AM System

Here the modulating signal s(t) with its DC component S is multiplied by the noise carrier y(t) to form the AM signal. The AM signal is detected in turn by a full wave square law device(2) and then is passed through a filter to recover the modulating signal, s(t).

(2) The term full-wave square law device is described in detail by Davenport and Root[4] by Eq. 13-13 on Page 280. The half-wave square law device is a more appropriate device to use as an optical detector. As Davenport and Root state on Page 302 the only difference between the two is a factor of 4, or 6 DB.

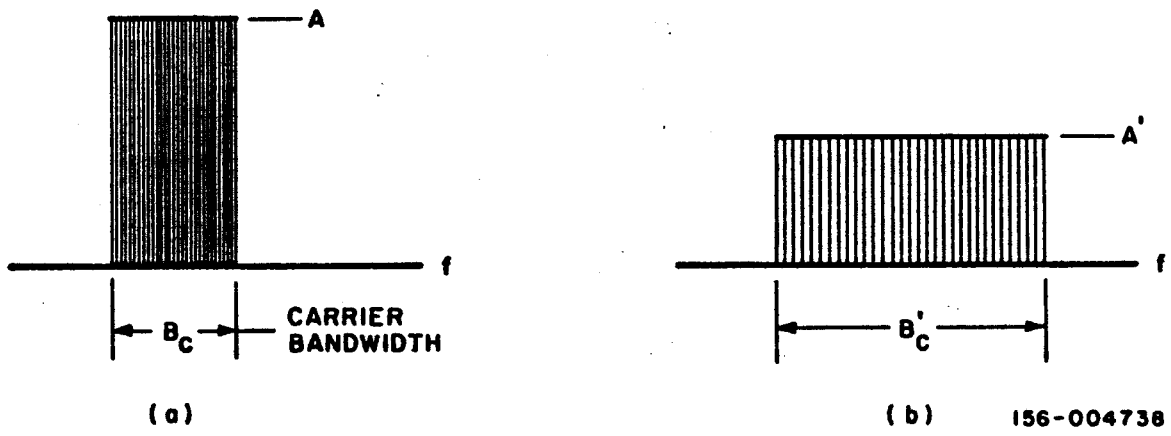

Figure 2. Different Spectral Densities But with Total Power Equal. (See text for explanation.).

The autocorrelation function of the output of the square law device is:

$$R_x(t_1, t_2) = E\left\{ \left[S + s(t_1)\right]^2 \; y^2(t_1) \; \left[S + s(t_2)\right]^2 \; y^2(t_2) \right\} \tag{1}$$

Assuming $s(t)$ and $y(t)$ are statistically independent and s, s^2, and y^2 are stationary and $E\left\{ s(t) \right\}$ is zero,

$$R_x(\tau) = S^4 R_{y^2}(\tau) + S^2 (2\sigma_s^2) R_{y^2}(\tau) + 4 S^2 R_s(\tau) R_{y^2}(\tau) + R_{s^2}(\tau) R_{y^2}(\tau) \tag{2}$$

The power spectrum is:

$$P_x(f) = \int_{-\infty}^{+\infty} R_x(\tau)\, e^{-j2\pi f\tau}\, d\tau \tag{3}$$
$$= \left[S^4 + 2\sigma_s^2 \; S^2\right] P_{y^2}(f) + 4S^2 P_{sy^2}(f) + P_{s^2y^2}(f)$$

As Rowe did, let the spectral density of the noise carrier have Gaussian characteristics,

$$P_y(f) = \frac{1}{\pi\sqrt{\pi}\,B} \left\{ e^{-\left[\frac{f+fo}{B}\right]^2} + e^{-\left[\frac{f-fo}{B}\right]^2} \right\}, \quad B \ll fo \tag{4}$$

and the baseband modulating signal be,

$$P_s(f) = \begin{cases} \frac{1}{2W}, & |f| < W \\ 0, & |f| > W \\ S, & f = 0 \end{cases} \qquad W \ll fo \tag{5}$$

It can be shown,

$$P_{y^2}(f) = \left[\frac{2}{\pi}\right]^2 \delta(f) + \frac{2}{\pi^2\sqrt{2\pi}\,B}\left\{e^{-\frac{1}{2}\left[\frac{f+2fo}{B}\right]^2} + 2\,e^{-\frac{1}{2}\frac{f^2}{B^2}} + e^{-\frac{1}{2}\left[\frac{f-2fo}{B}\right]^2}\right\} \quad (6)$$

Also

$$P_{s^2}(f) = S^2\,\delta(f) + 2\int_{-\infty}^{\infty} P_s(f')\,P_s(f-f')\,df' \quad (7)$$

$$= \begin{cases} 2\left\{\frac{1}{2W}\right\}^2(2W-f), & f > 0 \\ 2\left\{\frac{1}{2W}\right\}^2(2W+f), & f < 0 \end{cases}$$

$$P_{s^2y^2}(f) = \int_{-\infty}^{\infty} P_{s^2}(f')\,P_{y^2}(f-f')\,df' \quad (8)$$

After neglecting terms centered about $\pm$ 2fo,

$$P_{s^2y^2}(f) = \frac{2W-f}{2W^2}\left[\frac{2}{\pi}\right]^2 + \frac{2\sqrt{2}\,S^2}{\sqrt{\pi}\,\pi^2\,B}\,e^{-\frac{f^2}{2B^2}}$$

$$+ \frac{B}{\pi^2 W^2}\sqrt{\frac{2}{\pi}}\left[e^{-\left\{\frac{f^2}{2B^2}\right\}} - e^{-\frac{1}{2}\left\{\frac{f+2W}{B}\right\}^2}\right]$$

$$+ \frac{1}{\pi^2 W}\left\{2 - \frac{f}{W}\right\}\left[\operatorname{erf}\left\{\frac{f+2W}{\sqrt{2}\,B}\right\} - \operatorname{erf}\left\{\frac{f}{\sqrt{2}\,B}\right\}\right] \ldots f \leq 0 \quad (9)$$

$$P_{s^2y^2}(f) = \frac{2W+f}{2W^2}\left\{\frac{2}{\pi}\right\}^2 + \frac{1}{\pi^2 W}\left\{2 + \frac{f}{W}\right\}\left[\operatorname{erf}\left\{\frac{f}{\sqrt{2}\,B}\right\} - \operatorname{erf}\left\{\frac{f-2W}{\sqrt{2}\,B}\right\}\right]$$

$$+ \frac{\sqrt{2}\,B}{\sqrt{\pi}\,\pi^2 W^2}\left[e^{-\frac{1}{2}\frac{f^2}{B^2}} - e^{-\frac{1}{2}\left\{\frac{f-2W}{B}\right\}^2}\right] \quad \ldots\ldots\ldots\ldots f > 0$$

$$P_{sy^2}(f) = \int_{-\infty}^{\infty} P_s(f') \, P_{y^2}(f-f') \, df' \tag{10}$$

Again neglecting terms centered about $\pm 2fo$

$$P_{sy^2}(f) = \left[\frac{2}{\pi}\right]^2 P_s(f) + \frac{1}{\pi^2 W} \left\{ \operatorname{erf}\left[\frac{f+W}{\sqrt{2}\,B}\right] - \operatorname{erf}\left[\frac{f-W}{\sqrt{2}\,B}\right] \right\} \tag{11}$$

Combining equations (3), (6), (9), and (11) results in the full wave square law device output power spectral density, $P_x(f)$. Removing the $P_s(f)$ term from $P_x(f)$ will leave that part of $P_x(f)$ which contains noise terms only. Integrating this expression from -W to +W which is the low pass filter passband will give the noise output power and dividing by the coefficient of the $P_s(f)$ term will give the noise-to-signal power as a function of $\frac{W}{B}$. Assuming the DC part of the modulating signal to be 3, i.e., S = 3, as Rowe does and omitting the DC term in the output because it does not contain the modulating signal results in the following expression for noise-to-signal ratio.

$$\frac{N}{S} = \frac{1}{36} \left\{ \frac{38}{\sqrt{2\pi}} \frac{B}{W} + \frac{1}{2} \left[747 + \frac{B^2}{W^2}\right] \operatorname{erf}\left[\frac{1}{\sqrt{2}} \frac{W}{B}\right] \right. \tag{12}$$

$$+ \left[39 - \frac{1}{4} \frac{B^2}{W^2}\right] \operatorname{erf}\left[\frac{\sqrt{2}\,W}{B}\right] - \frac{1}{\sqrt{2\pi}} \frac{B}{W} e^{-\frac{1}{2}\frac{W^2}{B^2}}$$

$$\left. + \frac{39}{\sqrt{2\pi}} \frac{B}{W} e^{-2\frac{W^2}{B^2}} \right\}$$

Figures 4 and 5 show this equation plotted. Also shown is Rowe's linear detector curve for the baseband case.

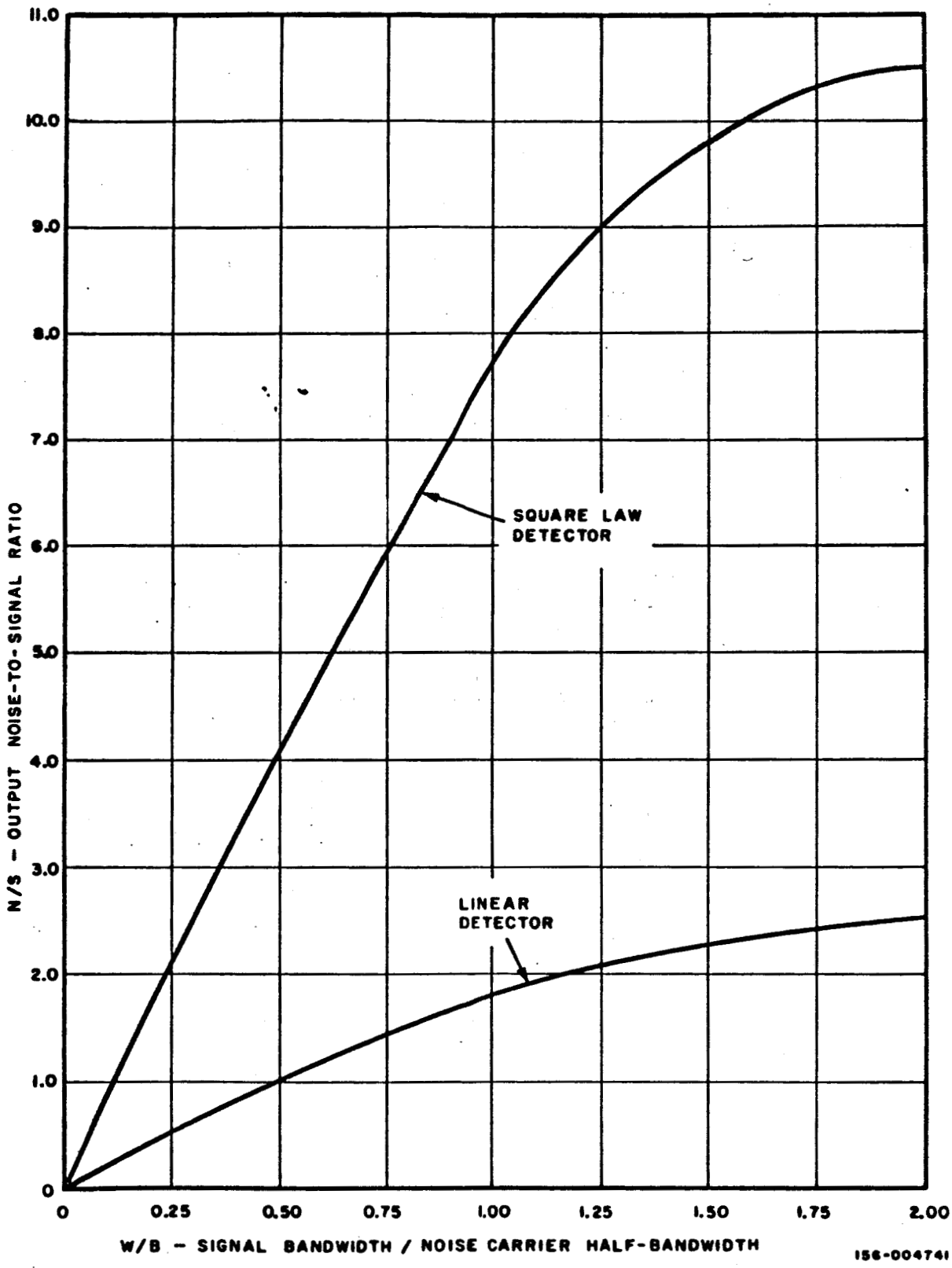

Figure 4. Comparison of Full-Wave Square Law Detector and Rowe's Linear Detector for Baseband Modulation

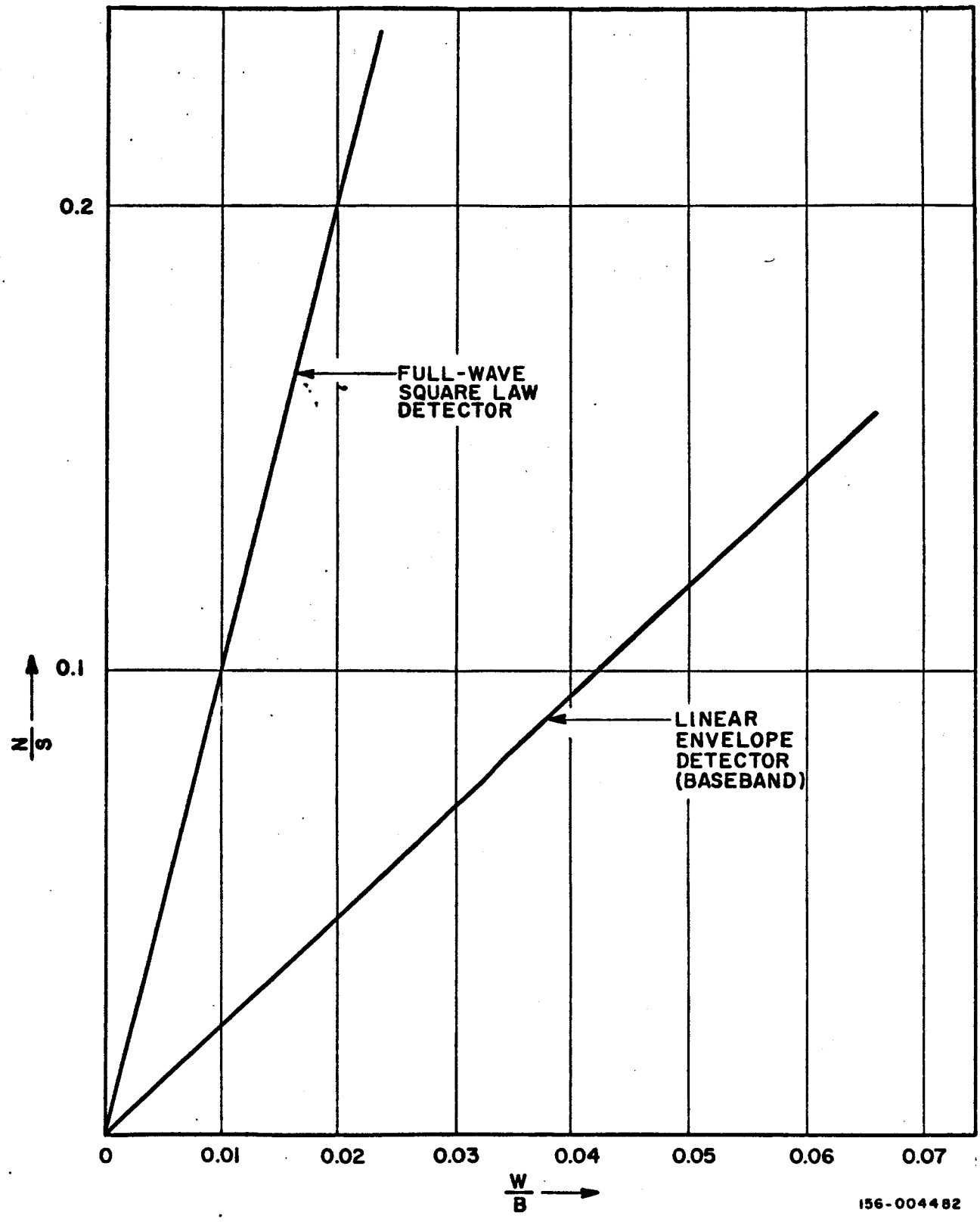

Figure 5. Effect of Noise Carrier Bandwidth

1.2.3 Summary of Noise Sources

It is evident that noise sources in laser systems can be numerous. The list below summarizes the noise sources and indicates the variety of considerations that must be given to a laser receiving system in order to minimize the total noise.

a) Noise-In-Signal (quantum noise)	Statistical fluctuations of signal power
b) Background radiation noise	Statistical fluctuations of background radiation
c) Internal noise due to dark current	Statistical fluctuations of current carriers or photoelectrons
d) Noise due to laser local oscillator power	Statistical fluctuations of local oscillator

Noises a, b, c, d all are different types of shot noise

e) Internal noise such as $1/f$ noise and current noise	Noise values dependent on device due to imperfections of detector
f) Noise due to non-coherent or quasi-coherent carriers	Noise dependent on carrier bandwidth and information bandwidths due to detection action
g) Noise due to non-ideal local oscillator	Noise due to beats between components of local oscillator with each other or signal due to finite noise bandwidth of local oscillator
h) Extra noise from laser source	Possible to occur due to high degeneracy of source
i) Modulation or tracking scintillation noise	Noise due to unwanted variation in background or signal average values.

The shot noise formula

$$i_n^2 = 2qiB$$

applies to a, b, c, d noise types where i is the particular current.

For noise-in-signal

$$i = i_s = \frac{\epsilon q P_s}{hf}$$

For background radiation noise

$$i = i_b = \frac{\epsilon q P_b}{hf}$$

For internal noise

$$i = i_d, \text{ the dark current}$$

For shot noise due to local oscillator power

$$i = i_{LO} = \frac{\epsilon q P_{LO}}{hf}$$

Where P_s, P_b and P_{LO} are the received signal power, received background power and the laser local oscillator power respectively.

The shot noise is essentially flat with bandwidth up to the post-detection bandwidth response of the detection system.

Dominant at low baseband frequencies is flicker or 1/f noise. Noise spectrum decreases with increasing frequency. Current noise is the analog of flicker noise in tubes. It has also been called contact noise, excess noise, modulation noise, and has sometimes been used to include all types of noise which depend upon bias current including g-r noise. Current noise, in general, can be described by

$$i_n^2 = \frac{C_2 i^{\alpha} B}{f^{\beta}}$$

where C_2 is a constant

β = 1.0-1.5 for current noise

α = is a constant from 1.25 to 4

Noise due to non-coherent carrier is discussed in sections 1.21 and 1.22. Extra or excess noise from a laser source is also discussed in 1.21.

Noise due to non-ideal local oscillation can be understood by reference to figure 6. If the local oscillator has a finite bandwidth it is possible for the components of the local oscillator to beat with itself and generate beats at the IF which is $|f_{LO} - f_s|$. These beats will compete with the signal. Since the local oscillator may be very much stronger than the signal in low level receiving applications, the spectral width at which these effects can occur may be very wide. The bandwidth of concern for the local oscillator may be the 50 DB points rather than the customary 3 DB. In addition to this noise, if the local oscillator 3 DB bandwidth is wider than the signal information bandwidth, the IF signal will be distorted due to mixing of the various local oscillator components with the signal components.

Modulation and/or tracking scintillation noise can be understood by noting that if changes in the average received energy occur that is not due to the signal modulation then these changes will result in additional detected noise. If these unwanted changes occur at the same frequencies as the signal modulation, the receiver cannot distinguish between it and the desired signal modulation. Thus systems have to be carefully examined to insure that such unwanted modulation does not occur at the signal modulation frequencies or if it does, it is of insufficient magnitude to be harmful. Further detailed treatment of this subject is required with complete mathematical analysis for various backgrounds, tracking rates, and modulation frequencies.

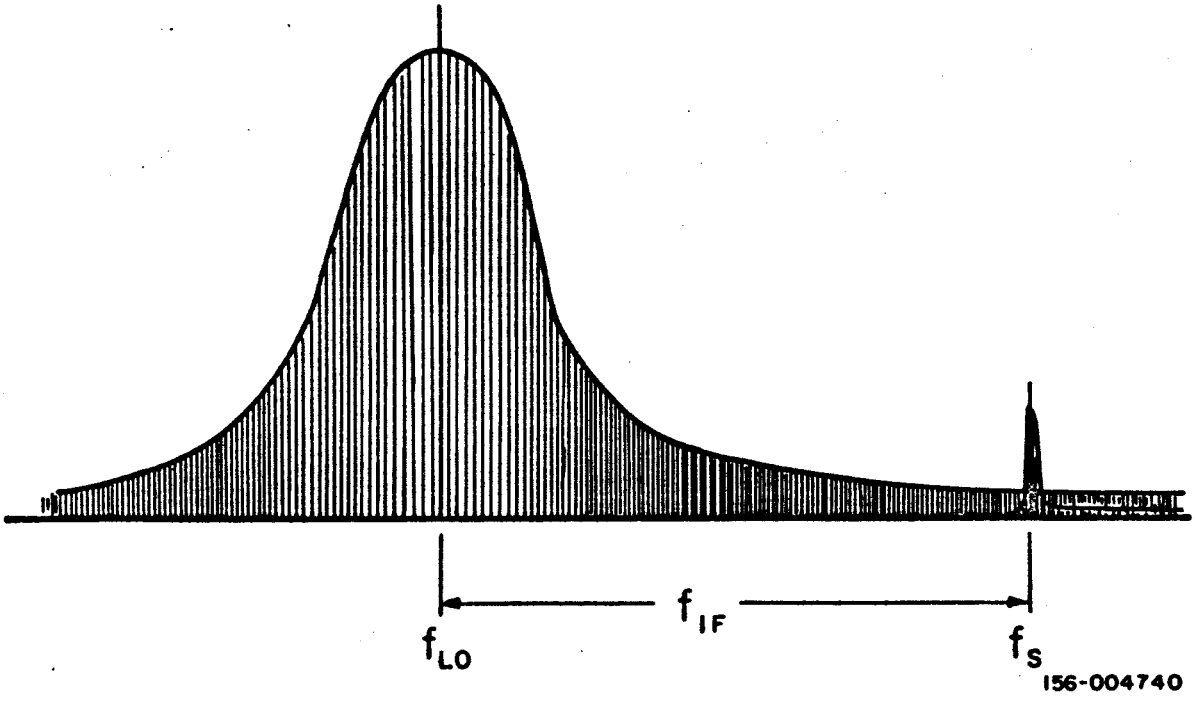

Figure 6. Non-ideal Local Oscillator and Signal Spectrum.

1.2.4 Information Theory Aspects

The quantum effects at optical frequencies must be considered in dealing with information theory considerations such as channel capacity of optical systems.

It is well established that without quantum considerations, that is, with the classical description of electromagnetic waves, the information capacity C of a signal in a channel is given by:

$$C = B \log \left(1 + \frac{S}{N}\right)$$

where:

B is the channel bandwidth

S is the average signal power

N is the additive white noise power

C will be in units of bits per second, the most common information unit, if the logarithm is taken to the base 2.

In order to realize this capacity limit, the signal must be coded in such a way as to have the statistical randomness of white noise.

The amount of uncertainty or entropy in a message is denoted by H and is given as:

$$H = - \sum_{i=1}^{M} P_i \log P_i$$

where:

P_i is the probability of occurrence of an event E_i

The greater the uncertainty about the message contents prior to receiving it, the greater the information thus conveyed when the message is received.

When all the possibilities are equally likely:

$$H = \log M$$

and is a maximum for the M possibilities.

The information rate, R, is given by:

$$R = HB$$

This can be said more explicitly to be the rate of arrival of entropy at the receiver.

The information capacity, C, in the presence of noise arises from two terms, the entropy rate for signal plus noise and the entropy rate for noise alone. That is, the information in the signal cannot be greater than the entropy of the combination of signal plus noise less the information less entropy of the noise alone.

Thus:

$$C = R\,(P = S+N) - R\,(P = N)$$

C is a maximum when S has the characteristic of noise. For the classical electromagnetic case,

$$R\,(P = S+N) = B \log \frac{S + N}{P_o}$$

$$R\,(P = N) = B \log \frac{N}{P_o}$$

P_o being an arbitrary constant upon use of the two rate equations to find the information capacity C, one obtains the basic information capacity formula $B \log (1 + \frac{S}{N})$.

If we followed this equation to its limit as S/N approached infinity, the information capacity would approach infinity. This cannot occur, however, because of the uncertainty principle. We cannot measure to any desired accuracy because of the uncertainty principle. We become limited as the noise approaches zero by fundamental quantum considerations. Thus, when we consider quantum effects, this equation can no longer be considered valid as it stands.

A derivation of channel capacity with consideration of quantum effects has been recently accomplished. The entropy per mode for white noise was determined to be:

$$H = \log (1 + \bar{m}) + \bar{m} \log (1 + \frac{1}{\bar{m}})$$

where $\bar{m}$ is the average number of photons in a mode. The energy per mode $\bar{E}$ is then $hf\bar{m}$. In bandwidth B, the incident power is given by

$$P = \bar{E}\,B = hf\bar{m}B$$

By substituting for $\bar{m}$ we obtain:

$$H = \log (1 + \frac{P}{hfB}) + \frac{P}{hfB} \log (1 + \frac{hfB}{P})$$

The information or entropy rate will then be given by:

$$R = HB = B \log \left(1 + \frac{P}{hfB}\right) + \frac{P}{hf} \log \left(1 + \frac{hfB}{P}\right)$$

Noting the C is $R_{(S+N)} - R_{(N)}$ we can write for the upper limit of information capacity

$$C = B \log \left(1 + \frac{S}{N + hfB}\right) + \frac{S+N}{hf} \log \left(1 + \frac{hfB}{S+N}\right) - \frac{N}{hf} \log \left(1 + \frac{hfB}{N}\right)$$

where N shall be considered as the additive white noise. If we defined N as the background from a black body at temperature T_N, then:

$$N = hfB \frac{1}{e^{hf/kt} - 1}$$

Figure 7 illustrates the resultant maximum information capacity in bits/second for different power levels as a function of frequency for $T_N = 290^{\circ}K$ and $B = 10^9$ CPS.

If N is considerably greater than hfB (the number of photons per mode is much greater than one) we obtain

$$C = B \left[\log \left(1 + \frac{S}{N}\right) - \frac{hfBS}{2N\,(S+N)} \log e \ . \ . \ . \right]$$

Since $N >> hfB$, the second term is always much smaller than the first and the equation for the classical condition is obtained.

If we assume $N << hfB$, we find

$$C = B \log \left(1 + \frac{S}{hfB}\right) + \frac{S+N}{hf} \log \left(1 + \frac{hfB}{S+N}\right) - \frac{N}{hf} \log \left(\frac{hfB}{N}\right)$$

For $Y = e^{hf/kt} - 1$

When $S >> N$, this reduces to, since $\bar{m} >> \frac{1}{Y}$,

$$C = B \left[\log \left(1 + \bar{m}\right) + \bar{m} \log \left(1 + \frac{1}{\bar{m}}\right) - \frac{1}{Y} \log Y \right]$$

The first two terms depend only on $\bar{m}$, which is the ratio of average signal power to hfB ratio. The last term is negative and depends on the ratio hf/kt. For a given optical frequency, f, this term depends solely on the background temperature T.

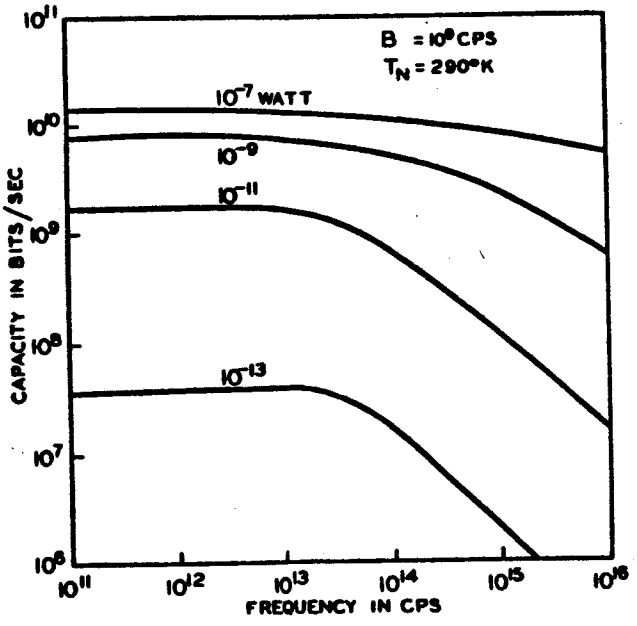

Figure 7. Upper limit to the information that may be incorporated into an electromagnetic wave in a single transmission mode. Thermal noise, as originating from a black body at 290°K, is assumed to accompany the wave.

The channel capacity is constituted of two independent parts, one dependent on the average signal power to hfB ratio and the other dependent on black body noise.

The two parts are plotted separately in two figures. Only for very high temperature is the reduction in channel capacity due to this black body noise significant.

For above figures and expressions for $N << hfB$ to be valid $S >> N$ but N is a function of T. Figure 8 shows regions of validity.

The information capacity will be affected by the optical receiver configuration in that the effective input noise of the receiver will help determine the total noise power.

The linear amplifier reduces the capacity to that of:

$$C_{amp} = B \log \left(1 + \frac{S}{N + KhfB}\right)$$

where $K \geq 1$

We can define information efficiency of the quantum amplifier as the ratio of $C_{amp}/C_{max.}$ where $C_{max.}$ is the theoretical maximum. For the ideal linear amplifier of $K = 1$, Figure 9 illustrates the situation for various values of signal, $T_N = 290^{o}k$ and $B = 10^{9}$ CPS. Note the rapid drop-off in efficiency at optical frequencies and low signal powers. This is to be expected since hfB becomes more significant under these conditions.

The photomixing or heterodyne receiver effect on the channel capacity has been determined to be:

$$C_{het} = B \log \left(1 + \frac{S}{N + \frac{hfB}{\epsilon}}\right)$$

It should be noted that N is the additive input noise over the bandwidth B which is the IF bandwidth. In the photomixing receiver, the major shot noise contribution is due to the local oscillator power, and only the background power that is in the optical signal spectrum (so that it is transferred to the IF bandwidth) will be significant as a background noise contribution.

In homodyne operation (zero frequency IF or baseband operation after photomixing), the information capacity is given by

$$C_{hom} = \frac{B}{2} \log \left(1 + \frac{2S}{N + \frac{hfB}{2\epsilon}}\right)$$

N is the background power received in the optical band B, and the detection bandwidth need be only B/2.

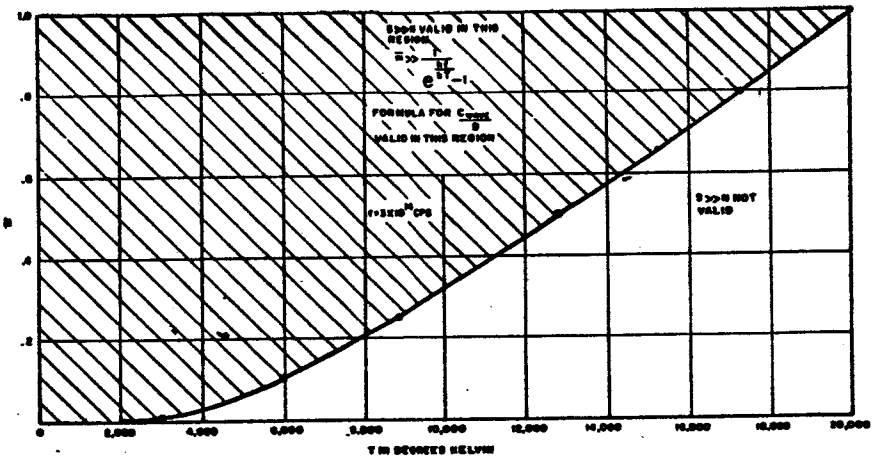

Figure 8. Regions of Validity for $\frac{C_{wave}}{B}$

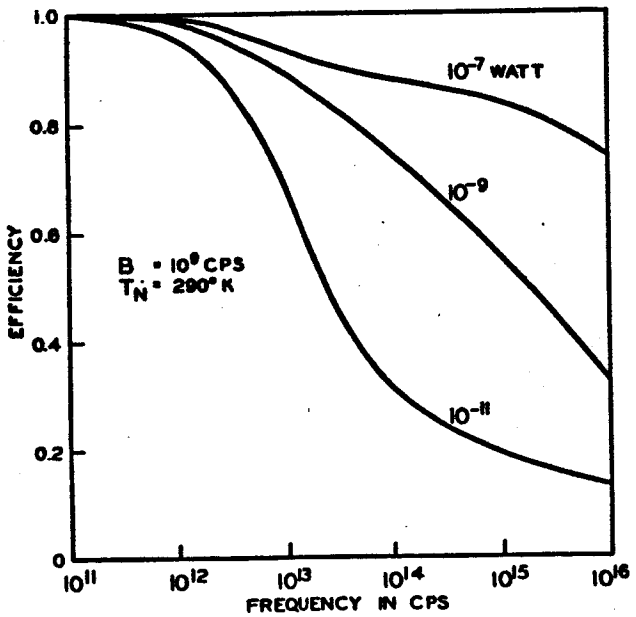

Figure 9. Information efficiency for an ideal amplifier of high gain. Because of spontaneous emission, the ideal amplifier has an effective input noise power of hvB, which is responsible for the lowering of its efficiency at high frequencies.

For the quantum counter case, that is a receiver in which photoelectrons are counted as they are produced from the incident signal, interesting differences from the other cases appear.

For large received $\bar{n}$ in the quantum counter case,

$$I_p = \frac{C}{\bar{n}} = \frac{1}{2\bar{n}} \log (1 + k^2 \bar{n})$$

where k is the modulation factor and is small, I_p is the photon information rate.

If we include background,

$$I_p = \frac{1}{2\bar{n}} \log (1 + \frac{k^2\bar{n}^2}{\bar{n} + \bar{n}_b})$$

In general, the information, I, is determined to be

$$I = \frac{C_{counter}}{B} = -P_t(1)\,(1-e^{-\bar{n}}) \log p_t\,(1)$$

$$- \left[1 - P_t(1)\,(1-e^{-\bar{n}}) \right] \log \left[1 - P_t(1)\,(1-e^{-n}) \right]$$

$$+ P_t(1)\, e^{-\bar{n}} \log e^{-n}$$

If we hold average power constant, the maximum information per symbol can be found by the transcendental equation

$$\log_e \left[\frac{\bar{n}}{\bar{n}_r} + e^{-\bar{n}} - 1 \right] = \frac{\bar{n}}{(e^{\frac{\bar{n}}{\bar{n}+1}} - 1)}$$

Figure 10 plots this equation and gives the maximum information conditions for $\bar{n}$ and $\bar{n}_r$. Example: If we have average photons received per interval of about $\bar{n}_r = 1.6$, the maximum information capacity is attained for pulse system when $\bar{n} = 4$ photons/received pulse. The system should be constructed and coded so that $P_t(1) = 1.6/4 = 0.4$.

At small values of $\bar{n}_r$, the curve levels off so that even at very low values of $\bar{n}_r$, the maximum information capacity will be obtained for average photons per received pulse not much less than one. This indicates that for low average signal levels, a pulse system of very low duty cycle will be more efficient.

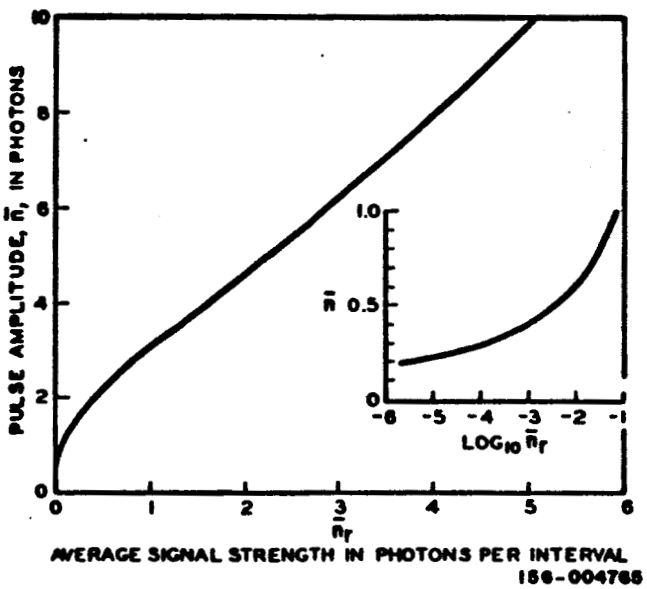

Figure 10. Optimized average received pulse amplitude for the noiseless binary channel as a function of the average number of received photons per available time interval. The probability of sending a pulse is given by $Q = \bar{n}_r/\bar{n}$.

For extremely small signals $\log_e \frac{1}{\bar{n}_r} >> 1$ and $I_{max} \rightarrow \bar{n}_r \log \frac{1}{\bar{n}_r}$

The addition of non-signal photoelectrons into the quantum counter system will not significantly affect results as long as the number of non-signal photoelectrons per 1/B interval is much less than the signal photoelectrons in the same interval.

The information efficiency $C_{counter}/C_{theoretical}$ is plotted.

Information efficiency as a function of non-signal photoelectrons for ratios of P/hfB is also plotted. The coherent amplifier efficiency is also plotted.

At low background and low internal noise, ($n_e << 1$) the quantum counter is more efficient. As n_e increases towards unity, the coherent amplifier shows greater potential efficiency.

When the average number of received photons per interval becomes much greater than unity (i.e., P>> hfB) the information capacity of the quantum counter approaches half the theoretical maximum capacity, or in words, the information efficiency approaches 0.5. For large number of photons per interval, the quantum considerations should not be significant. Further, it is known that, classically, equal amounts of information may be obtained from amplitude and phase measurements; thus, since the quantum counter throws away all phase information, it should be half as efficient as possible.

The information efficiency for the various receiver systems has been plotted in Figure 11 for a particular set of conditions of $T_N = 290^oK$, $P = 10^{-11}$ watts, $B = 10^9$ CPS.

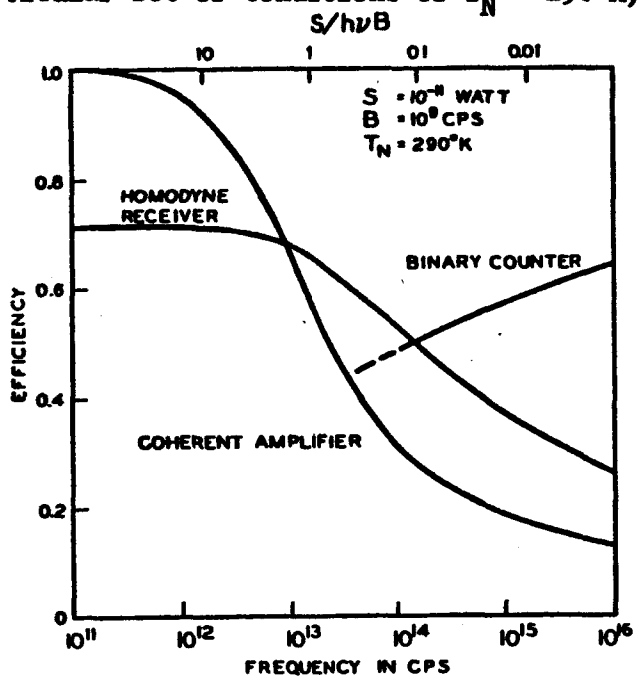

Figure 11. Information efficiency for various receivers for an average received signal power of 10^{-11}w, a bandwidth of 10^9 CPS, and an external noise temperature of 290^o. Note that at the higher frequencies the coherent amplifier is not as good as the other types of receivers.

1.3 New Technology

There are no reportable items within the meaning of the New Technology clause of NASA Form 417 (1-63) and Alteration dated November 1963.

1.4 Program For Next Reporting Period

In the next reporting interval, the following work will be accomplished on Task I. First, the case of a microwave sub-carrier on an optical carrier will be analyzed for its effects on detected signal-to-noise ratio in a square-law detector. Second, an analysis of photomixing and photodetection techniques will be included with emphasis on system considerations, theoretical and practical. The limitation of present receiving devices on photomixing and photodetection systems will be analyzed and areas of necessary improvement noted. A specific noise study of the dynamic-crossed-field electron multiplier will be undertaken in this report period.

1.5 Conclusions and Recommendations

It has been shown that there are many noise sources to be considered in laser systems; some can be minimized considerably by understanding their origin. It was shown that the noise bandwidth of the carrier and the information bandwidth of the signal are interrelated in determining the detected signal-noise ratio. This indicates that choice of a laser source will depend, in part, upon the bandwidth of the transmitted information. One cannot simply modulate a laser source and expect a reasonable signal-noise ratio without serious consideration of the carrier and information bandwidth factors.

Information theory aspects indicate that a low duty cycle pulse coding may be the most efficient transmission at optical frequencies. This does not necessarily mean a binary type code. A pulse position system with many possible positions may be desirable in that it could be very efficient.

In a system situation, each one of the noise sources should be examined to determine its particular effect on the overall signal-noise ratio. In so doing, one will be able to determine the system component specifications necessary for adequate system operation.

To accomplish this, it is necessary to study in detail such items as tracking and scintillation noise modulation and noise effects in amplitude modulation of quasi-laser carriers.

Improvement in system performance can be obtained by study of optimum thresholds to reduce error rates and optimum methods of coding for highest information efficiency.

All of the above should be examined with regard to system configurations for satellite-earth links. Because of the novel nature of laser communications and the many possible noise contributions, it is most important to examine all possible system aspects to eliminate undesirable configurations and optimize desirable configurations.

2. TASK II EFFORT

2.1 Introduction

Task II consists of a series of ten lectures, each four hours in duration to be presented by Mr. Monte Ross. The lectures, which shall deal with laser receivers and systems, shall include the subject matter of Task I. Five lectures were given in the second quarter.

2.2 Discussion

Five lectures were delivered by Mr. Monte Ross at Goddard Space Flight Center, Greenbelt, Maryland, during the period of 17 August to 21 August 1964. The subject matter of these lectures was as follows:

1. Radiation Laws and Statistics
2. Noise and Fluctuations
3. Detection Statistics
4. Information Theory Aspects

2.3 New Technology

There are no reportable items under Task II within the meaning of the New Technology clause of NASA Form 417(1-63) and Alterations dated November 1963.

2.4 Program for Next Reporting Period

The subject matter for the remaining five lectures under Task II will include Receiving Devices, Receiving Techniques, Receiving Systems, and Electro-Optic Devices.

2.5 Conclusions and Recommendations

It is deemed to be more beneficial to NASA to have the lecture material provided in the form of manuals which would be used as Textbooks by the attendees at the lectures. The manuals would contain lecture material for the first five lectures, as well as lecture material for the remaining five lectures to be given under Task II.

3. TASK III EFFORT

3.1 Introduction

Task III consists of developing and delivering one Dynamic Crossed-Field Electron Multiplying (DCFEM) light demodulator which is to be capable of a voltage signal-to-noise ratio of 3 DB when detecting 10^{-12} watts of 6321AU radiation with a modulation frequency of 3 KMC and a detection bandwidth of 1 KC.

The device incorporates many desirable features of static multipliers, such as low noise, exceptionally high amplification, and good spectral response; it has the additional advantage of providing wide signal bandwidth and a much simpler cathode and secondary emission structure. It has superior characteristics when compared with other available devices capable of detecting high frequency modulation.

This device is the first photomultiplier with microwave response. It enables use in instrumentation and scientific experiments where pulses of a nanosecond or less need to be detected in a sensitive manner.

The high sensitivity and large bandwidth of a microwave-bandwidth photomultiplier results in instrument capabilities not previously possible, and makes feasible laser systems for space communications and high-resolution radar.

The DCFEM can provide unsaturated outputs exceeding one MA, thereby eliminating the need for post detection amplification as well as linear and stable gain over a wide range of operating conditions.

A schematic diagram of the basic detector configuration is indicated in figure 12. This figure shows two electrodes incorporated in the high electric field region of a rectangular metal cavity resonant at 3 GC. Typical parameters for this configuration are an inter-electrode spacing of 3 MM, and an electric field intensity in the range of 10^5 to 10^6 volts/meter, providing eight multiplication stages. A microwave pump source of not more than a few watts is needed. The active electrode (secondary emission surface) is Beryllium-Copper, Magnesium Oxide or some other suitable material. A small area (20 MM^2) of the active electrode is covered with a photocathode chosen for the spectral response desired. An external magnet supplies a uniform field of about 500 gauss. The length of the column supporting the pedestal is chosen for either 1/4 or 3/4-wavelength resonance modes. It is to be noted that only three external electrical connections are required in contrast to the ten or more connections commonly required with electrostatic photomultipliers.

The electron multiplication in the detector is realized by providing a region in which there are two spatially uniform crossed fields. In figure 12 the static magnetic field points out of the plane of the paper, and the microwave electric field lies vertically in the plane. The region is bounded by two electrodes, one active electrode having a high secondary emission ratio, δ, and the other an inactive electrode or pedestal having a δ of less than unity. Incident light on the photocathode produces photoelectrons which are accelerated initially in the positive-x direction during the positive portion of the microwave voltage cycle. However, the magnetic field curves the paths as shown, and during the negative portion of the

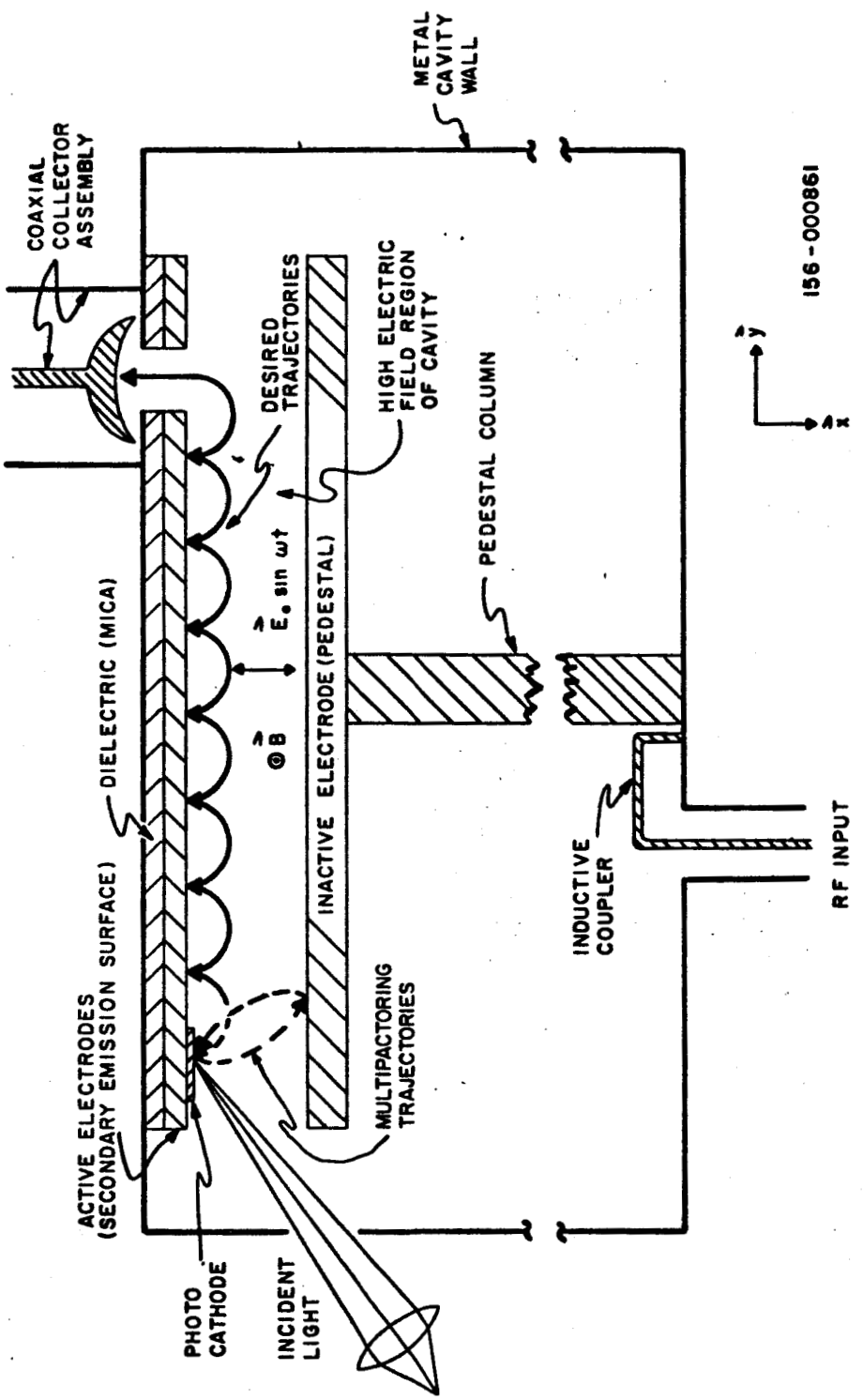

Figure 12. Schematic Diagram of Dynamic Crossed-field Electron Multiplier.

cycle the electrons impinge back onto the active electrode where they produce secondary emission electrons. Each of these secondaries is accelerated and curved back onto the active electrode, where additional secondaries are produced. This multiplication process is repeated for n stages, after which the electrons are collected by the coaxial collector assembly.

From preliminary work in the first quarter it was determined that for high vacuum purposes it would be an improvement to re-design the cavity in a cylindrical rather than rectangular geometry as shown in figure 13. This cylindrical geometry is smaller and easier to fabricate, assemble, and align and its electrical characteristics are as good as or better than the rectangular configuration.

Work in the second quarter has seen construction and evaluation of the cylindrical geometry tube. Results indicate good progress towards the objective.

3.2 Discussion

3.2.1 Tube Construction

A detector was brazed together in the vacuum furnace described in the last quarterly report. It is shown in figure 14. When the final brazing operation was completed the detector body was leak checked and a small leak was detected in the sapphire window. The sapphire to Kovar joint was then gold plated and again baked out in an attempt to seal the leak. This procedure failed. It was then decided that since the leak was small (10^{-6} mm-Hg) that it would be closed with low vapor pressure epoxy. This seemed preferable to discarding the tube body. The quarter wave, isolated, shorting section was inserted and the assembled tube was "baked out" on the vacuum pump. Upon completion of the "bake out" procedure it was discovered that the detector cavity indicated no resonance at 3000 MC as expected, and previously measured. When the device was removed from the vacuum pump and again tested, it exhibited the proper resonance response. After considerable testing and re-testing, it was determined that one part of the two piece quarter wave, isolated, shorting section had warped several thousandths of an inch and was not making proper electrical contact.

This section was repaired and re-assembled providing the expected resonance, however, the expected "Q" was also attributed to the warped section of the quarter wave shorting section.

An Antimony-Cesium photocathode was formed after the device was re-assembled, evacuated, and baked out. After the formation of the photocathode, an electromagnet was placed in the proper position and the RF drive was applied, as was the DC field.

The detector operated properly with 5 watts of input power at 3.125 KMC, 900 volts of DC and a 750 to 800 gauss magnetic field. The small signal current gain of the detector was 10^5 under these conditions. Additional gain could be obtained by increasing the RF power input, however, the device tended to be unstable and would occasionally multipactor.

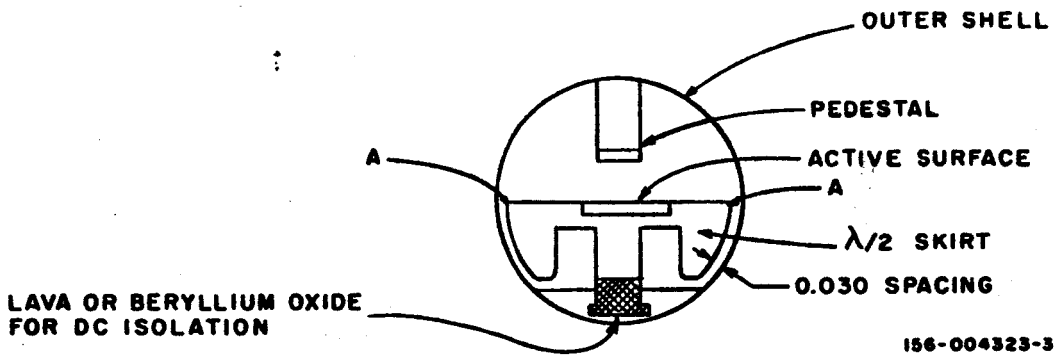

Figure 13. Cylindrical Cavity Using Non-Contacting Microwave Short Circuit.

Figure 14. DCFEM (Cylindrical Geometry).

The electron collection efficiency was measured and found to be between 70% and 80%. This was less than the 99% collection efficiency of the previous $3\lambda/4$ tubes. This reduction of collector efficiency is attributed to the fact that the collector in the present detector is about 0.050 inch below the dynode surface, whereas it was flush with the dynode surface in the old $3\lambda/4$ detector. This also accounts for the reduction of maximum current output at saturation. It was 4 milliamps compared to 6 milliamps on the $3\lambda/4$ detector. There is some evidence that the instability encountered at higher power levels may be involved with the uncollected electrons. This is thought to be a possibility since the $3\lambda/4$ detectors were stable with as much as 4 times the normal input power.

Two additional detector envelopes were brazed together during this reporting period. One of these leaked severely and was discarded. The other unit, it was found, had a loose collector, however, it is vacuum tight. Attempts are being made to replace the loose collector with one that will very nearly be flush with the dynode surface in order to collect the bulk of the electrons produced. In addition, all of the present $\lambda/4$ isolated shorting sections are of one piece construction in order to eliminate the earlier problems encountered. Cavities using the one piece shorting sections have exhibited "Q's" between 800 and 1000, which is desired.

3.2.2 Preliminary Measurement of Frequency Response of DCFEM

The frequency response of the detector was investigated using two methods of analysis. The first method involved beating together on the detector photocathode, the available excited modes in the output of a 6320 Å visible gas laser. The modes are separated by 150 megacycles corresponding to half wavelength longitudinal modes of the meter long resonator system used to excite the laser modes. The second method utilized the input light created shot noise of the detector.

The discernible beats obtained from the gas laser input ranged from 150 megacycles to 600 megacycles. The first two beats, 150 MC and 300 MC were detected on a Polarad spectrum analyzer, Model STU-1B equipped with a 10 MC to 1000 MC RF tuning head.

The output beats were photographed on a Polaroid camera attachment and are shown in figure 15. The 450 MC and 600 MC beats were detected with a NF 105 narrow band receiver tunable from 400 MC to 1000 MC. The receiver contained a signal strength meter, and relative measurements indicated that the 600 MC beat was 12 DB below the 450 MC beat. This result is consistent with theoretical predictions since the modes which produce the beats decay as in a Gaussian distribution. No attempt at this time was made to determine the bandwidth of the beat outputs, since they were considerably narrower than the IF bandwidths associated with the measuring equipment (less than 40 KC).

The results of the beat experiment indicate that the tube is capable of responding to and reproducing at the least, a frequency of 600 MC. Further work will attempt to reproduce beats higher than 600 MC. One approach may be to excite more longitudinal modes in the gas laser by using a different mirror configuration in the laser resonator. All the previous experiments were conducted with the most stable mirror configuration which produced the least number of excited laser modes.

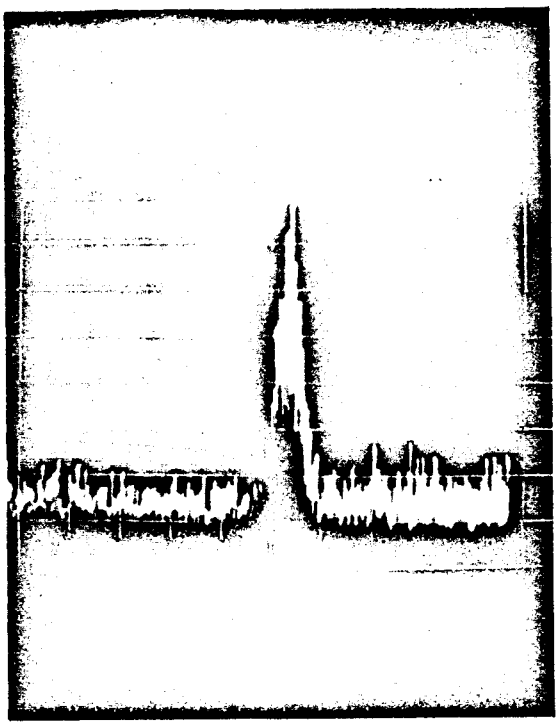

a. 150 MC

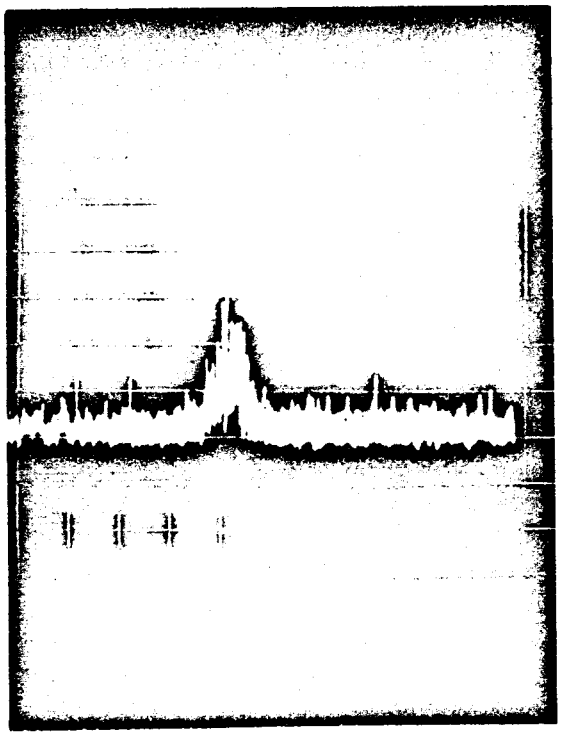

b. 300 MC

Figure 15. Laser Beat Frequencies Obtained from DCFEM Detector.

A larger number of modes would in effect distribute the available laser power more evenly between the output beats, decreasing the most prominent 150 MC beat, but also increasing the amplitude of higher frequency beats.

The shot noise method of determining frequency response involved measuring the noise output of the detector at various portions of the frequency spectrum. The base line noise of the receiver was measured by preventing any light energy from impinging upon the photocathode of the detector. Light induced shot noise was then displayed as increased amplitude from base line with the introduction of light energy. Measurements at 150 MC, 300 MC and 1000 MC were taken with the Polarad spectrum analyzer, and are shown in figure 16. The results indicated that the amplitude of the shot noise remained constant throughout the frequency band up to 1000 MC, which was the limit of the tuning head. In effect the results show: 1) that the output frequency characteristics of the detector are not degraded up to 1000 MC, and 2) amplification of frequencies up to 1000 MC occurs with a constant gain factor.

Additional work will be continued in the next period and will include the use of a 3000 MC modulator to amplitude modulate the input light signal. The detector will then operate in the heterodyne mode and mixing frequencies will be obtained.

3.3 New Technology

There are no reportable items under Task III within the meaning of the New Technology clause of NASA Form 417(1-63) and Alterations dated November 1963. It is expected that there will be reportable item(s) when concepts described in this report are first reduced to practice.

3.4 Program for Next Reporting Period

The program for the next reporting period will be to build a demountable tube for delivery to NASA. This device will be supplied with an external electromagnet to supply the required magnetic field and may also contain a 0.15 liter/second Vac-ion, appendage pump to maintain the required high vacuum.

Measurements of a more quantitative nature will be made to establish the device parameters.

3.5 Conclusions and Recommendations

Three DCFEM's with cylindrical geometry configuration were constructed and tested in the second reporting period. One was discarded, one is being modified, and one was operated to obtain preliminary data. Construction techniques developed for Task III appear adequate for experimental tubes, and preliminary data indicates that objectives are being met ahead of schedule.

It is recommended that the program for Task III be accelerated to permit delivery of the DCFEM ahead of schedule. This will permit use of this device in NASA's Optical Sensor Program at Goddard Space Flight Center at an advanced date and thereby accelerate NASA's overall objectives.

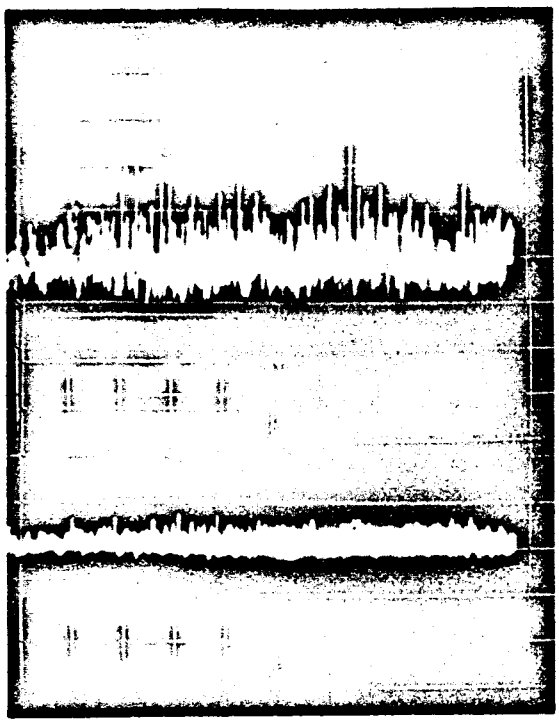

a. 150 MC

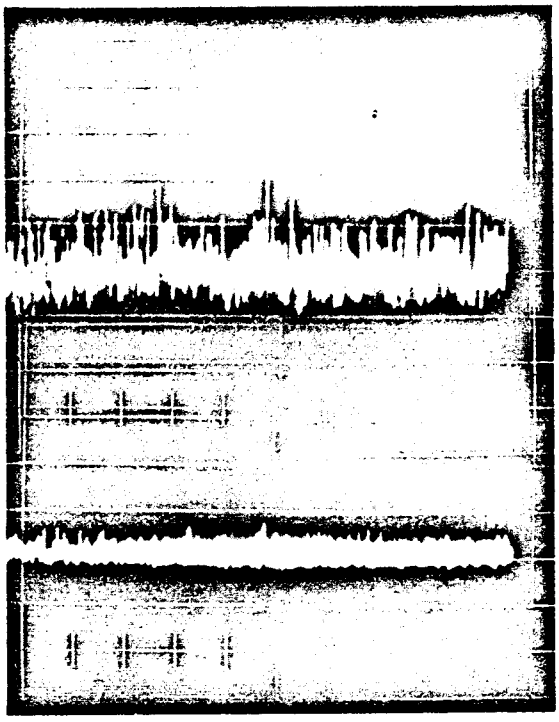

b. 300 MC

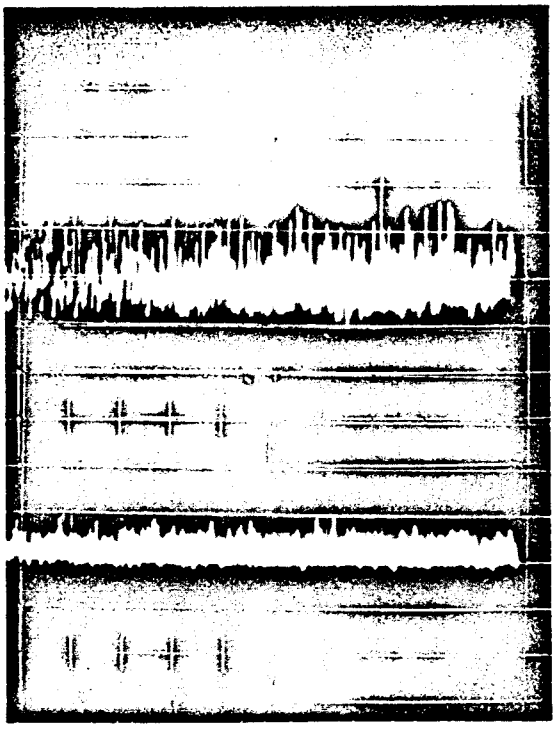

c. 1000 MC

Figure 16. Shot Noise Versus Base Line Noise at Various Frequencies (Upper trace is shot noise plus base line, lower trace is base line only).

It is further recommended that future work include the following:

1. Reduction of minimum microwave power input by reducing the step spacing and improvement of the cavity Q.

2. Improvement of the collector efficiency.

3. Improvement in design of the magnetic field so that the developed tubes should be complete with a light-weight permanent magnetic field.

4. Development of tubes with additional photosurfaces. Investigation of photosurfaces such as S-17, S-1 and S-20 should be accomplished.

BIBLIOGRAPHY

1. W. Fellgett, "Question of Correlation between Photons in Coherent Beams of Light," Nature, May 11, 1957.

2. L. P. Bolgiano, "Quantum Fluctuations in Microwave Radiometry," IRE Trans. on Microwave Theory and Techniques, July 1961.

3. H. E. Rowe, "Amplitude Modulation with a Noise Carrier," Proc. of the IEEE, Vol. 52, No. 4, pp. 389-395.

4. W. B. Davenport and W. L. Root, "Random Signals and Noise," McGraw-Hill, N. Y., N.Y., 1958.